AIChE InterScience DISCOVER SOMETHING GREAT

Co-synthesis of H_2 and ZnO by In-Situ Zn Aerosol Formation and Hydrolysis

Frank O. Ernst, Antonio Tricoli, and Sotiris E. Pratsinis
Particle Technology Laboratory, Swiss Federal Institute of Technology (ETH) Zurich, CH-8092 Zurich, Switzerland

Aldo Steinfeld
Institute for Energy Technology, ETH Zurich, CH-8092 Zurich, Switzerland, and Solar Process Technology, Paul Scherrer Institute, CH-5232 Villigen, Switzerland

DOI 10.1002/aic.10915
Published online June 21, 2006 in Wiley InterScience (www.interscience.wiley.com).

Simultaneous synthesis of H_2 and ZnO nanoparticles is investigated by steam-hydrolysis of Zn vapor in a hot-wall aerosol flow reactor with separated evaporation, cooling, and reaction zones. Superheated Zn vapor was carried by Ar into a tubular, quartz reactor where it was mixed and quenched by a superheated, equimolar H_2O/Ar stream, resulting in Zn/ZnO nanoparticles and H_2. The Zn(g) vapor was generated by electric heating of a Zn crucible whose weight was continuously monitored and compared to H_2 production rate. The reactor was operated at 1 bar and 573–1273 K: above and below the Zn saturation vapor pressure suppressing and allowing, respectively, Zn aerosol formation by condensation taking place in parallel with the omnipresent ZnO formation by gas phase or surface hydrolysis of Zn. The process yielded up to 90% H_2 conversion and nanoparticles with Zn and ZnO mean crystallite sizes of 100 and 40 nm, respectively, containing up to 80 wt % ZnO. © 2006 American Institute of Chemical Engineers *AIChE J,* 52: 3297–3303, 2006

Keywords: hydrogen, zinc, zinc oxide, nanoparticle, aerosol reactor, hydrolysis, solar energy

Introduction

Formation of H_2 by thermal dissociation of water on metals is the exothermic second step of the so-called two-step water-splitting cycles for storage and use of solar energy, the first of which is the endothermic reduction of metal oxides to metals using concentrated solar energy.[1] These metal-oxide cycles are the promising high-temperature technologies for solar–thermal water splitting, as reviewed by Perkins and Weimer.[2] In particular, the hydrolysis of Zn to ZnO with release of H_2 is most attractive for its potential in achieving high energy conversion efficiencies.[3] Indeed rather recently strong international interest (including the U.S. Department of Energy) has been developed in such cycles for broader use of solar energy.[4]

Hydrogen formation by Zn vapor hydrolysis, however, has been reported in hot-wall aerosol reactors resulting in ZnO deposition on the reactor walls, making ZnO recovery and recycling rather difficult.[5] Hydrogen was also produced at high conversion by bubbling steam through a Zn melt,[6] a batch process that is demanding to implement because molten Zn gradually transforms to a Zn/ZnO composite that is difficult to process and regenerate. Very recently, H_2 has been produced continuously in hot-wall aerosol flow reactors by evaporating and subsequent in-situ hydrolyzing of Zn with a conversion rate of 70% with respect to the limiting reactant, Zn.[7] There, it was shown that along the reactor walls uniform XRD–pure ZnO films were formed at reactor temperatures above the Zn saturation temperature, whereas filamentary particles contain-

Correspondence concerning this article should be addressed to S. E. Pratsinis at pratsinis@ptl.mavt.ehtz.ch.

ing both Zn and ZnO crystallites were formed below that temperature. Pure Zn particles (130 nm crystallite size) were produced from the reactor, given that rather short residence times were used for their conversion to ZnO. In the cited works, local proximity of the temperature zones led to overlaid evaporation, particle formation, and hydrolysis.

Besides recycling ZnO in this solar cycle, ZnO particles find applications as vulcanizing agents and to a lesser extent as semiconductors, catalysts, cosmetics, and food supplements.[8] Note that ZnO is the third largest aerosol-made commodity by volume[9] produced by the so-called French and American processes,[8] leading to micron-sized particles that are used mostly as vulcanizing agents for tires. Typically ZnO nanoparticles, as used in electronics, optics, and photonics, are produced by wet-phase processes.[10] An overview on ZnO nanoparticle production by aerosol processes, with particle sizes in the range of 10–400 nm, is given by Tani et al.[11]

Here, hot-wall aerosol reactor synthesis of H_2 at high yields and simultaneous production of ZnO nanoparticles are explored in detail. This is of prime interest in solar engineering and promising for co-synthesis of H_2 during manufacture of fine oxide particles from their metal vapors. For this, a new aerosol reactor is assembled with separately heated Zn evaporation and hydrolysis sections. The Zn evaporation is monitored gravimetrically, whereas hydrogen production is monitored by gas chromatography at well-defined process temperatures and Zn(g) mass flow rates. It should be noted that this is a particularly challenging process because both H_2 and Zn/ZnO particle formation take place simultaneously by Zn condensation and hydrolysis in the gas or on the particle surface. By judiciously operating the reactor below or above its Zn saturation vapor pressure through temperature control of the reaction zone, however, it is possible to decouple Zn condensation from hydrolysis in the reaction zone itself. Furthermore, product particle characteristics are analyzed by X-ray diffraction, nitrogen adsorption, and microscopy relating them to process operation.

Experimental

Apparatus

Figure 1 shows a schematic of the vertical hot-wall aerosol flow reactor (a 5.5 cm inner diameter, 170 cm long quartz tube), consisting of three zones for metal evaporation, cooling, and hydrolysis. The evaporation zone containing an Al_2O_3 crucible initially loaded with Zn was heated by a concentric cylindrical electric furnace to the desired evaporation temperature, T_E. This crucible is supported by an Al_2O_3 rod resting on a balance, thus allowing for on-line monitoring of the zinc evaporation rate. An Ar (PanGas, 99.999% purity) stream carried Zn(g) from the evaporation zone through the cooling zone (L_C = 1 or 17 cm) into the reaction zone where it was T-mixed with H_2O–Ar flow from a steam generator (Bronkhorst CEM). The reaction zone was heated to temperature T_R by a second concentric cylindrical electric furnace. Product particles were collected downstream on a glass-fiber filter (Whatmann GF/A, diameter 150 mm), whereas excess steam was condensed in a water trap further downstream.

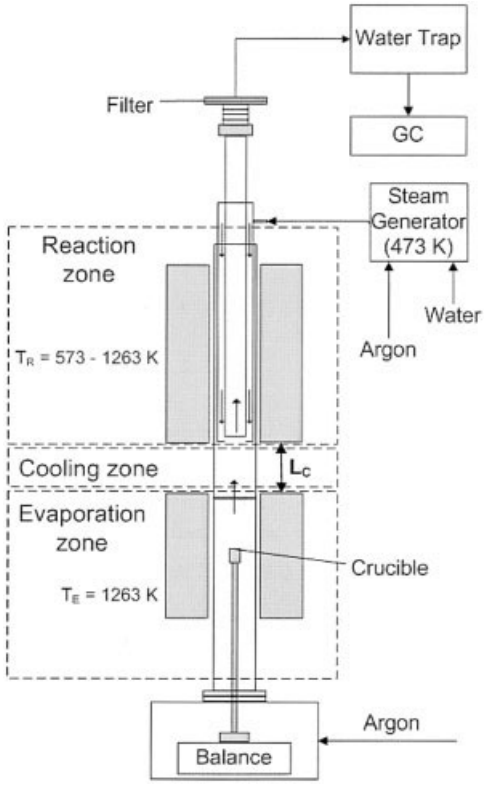

Figure 1. Apparatus for co-synthesis of H_2 and Zn/ZnO particles by in-situ formation and hydrolysis of Zn aerosol, featuring distinct evaporation, cooling, and reaction zones where the high temperature particle residence time can be controlled separately.

Procedure

Before heating the units, the crucible was loaded with about 3 g of zinc granules (Riedel-de-Haen, 99.99% purity). The two furnaces were heated to their set temperatures under Ar flow until the desired H_2O–Ar flow was injected in the reaction zone. After complete Zn evaporation, the reactor was kept at the same operational conditions for an additional 5 min before switching off gas flows and furnaces. After each experimental run, the reactor was disassembled, cleaned with diluted hydrochloric acid, and rinsed with deionized water.

For all experiments the following parameters were kept constant: T_E = 1263 K, carrier Ar gas flow rate Q_E = 2 L/min, and reaction gas (50% Ar and 50% H_2O vapor superheated to 473 K) flow rate Q_R = 2 L/min (L = liters at normal conditions; mass flow rates are calculated at 273 K and 1 bar). Two sets of experiments were performed to study the influence of the temperature profile on H_2 synthesis and Zn/ZnO product particle characteristics. In the first set, the cooling zone length was L_C = 17 cm and T_R ranged from 573 to 873 K, whereas in the second set, L_C = 1 cm and T_R = 923–1273 K. Varying the cooling zone length L_C allows for the investigation of ZnO formation not only at various reactor temperatures but also in the presence (high L_C) and absence (low L_C) of Zn particles formed by nucleation and condensation before their hydrolysis. Centerline temperature profiles in the evaporation, cooling, and

reaction zones were measured at the same flow conditions as for the actual experiments but without Zn. For this, a 750 mm long S-type thermocouple with a 0.5 mm bead shielded from thermal radiation with a 4 mm diameter alumina tube[12] was introduced from the end of the reaction zone.

The Zn partial pressure P_{Zn} is calculated from the Zn volumetric evaporation rate Q_{Zn}, the overall pressure P, and the gas flow rates:

$$P_{Zn} = \frac{Q_{Zn}}{Q_{Zn} + Q_E + Q_R} P$$

The equilibrium vapor pressure is given by[13]

$$\log P_{Zn,S} = 20.31 + \frac{4336}{T} + 10.07 \log T + 3.81 \times 10^{-3} T + 4.89 \times 10^{-7} T^2$$

The saturation temperature is defined as the temperature where the Zn partial pressure is equal to its equilibrium vapor pressure at that temperature and concentration before any Zn condensation has taken place. The saturation temperature is extracted iteratively.

Product characterization

The composition of the effluent gas and in particular the H_2 signal, after filter and water trap, was measured by gas chromatography (GC, Agilent). The specific surface area (SSA) of the collected particles on the filter was determined by nitrogen adsorption at 77 K (Micrometrics Gemini 2306) using the Brunauer–Emmett–Teller (BET) isotherm. Before this measurement, all samples were outgassed at 150°C for 1 h. Assuming all particles to be monodisperse spheres, the BET-equivalent particle diameter was calculated as $d_{BET} = 6/(\rho_{Zn/ZnO} SSA)$, with $\rho_{Zn} = 7140$ kg/m^3 and $\rho_{ZnO} = 5606$ kg/m^3. Phase composition and crystallite sizes of Zn, d_{Zn} (ICSD #64990[14]) and ZnO, d_{ZnO} (ICSD #34477[15]) were determined from X-ray diffraction (XRD) patterns (Bruker AXS D8 Advance, 40 kV, 40 mA) by the Rietveld method.[16] The particles were also examined by transmission electron microscopy (TEM) with a Zeiss microscope 912 Omega with ProScan and slow scan charge-coupled device (CCD) camera at 100 kV. All characterizations were carried out immediately after synthesis to avoid further oxidization, although this is limited for Zn at room temperature.[17]

The reactor performance is described by the overall chemical conversion X, the molar ratio of the H_2 produced to the Zn evaporated ($Zn + H_2O \rightarrow ZnO + H_2$), and by the effective particle yield Y, the molar ratio of Zn collected on the filter to the Zn evaporated from the crucible.

Results and Discussion

Reactor temperature profiles

Figure 2 shows the temperature profiles along the axis of the aerosol flow reactor for the two sets of experiments: $T_R = 623$ K with $L_C = 17$ cm (set 1, circles) and $T_R = 973$ K with $L_C = 1$ cm (set 2, triangles). In both sets, the temperature profiles in the evaporation zone are identical. The temperature of the Zn-containing crucible is 1263 K, which is above the Zn boiling point of 1180 K.[18] In set 1, the temperature drops steeply in the long cooling zone, reaching a minimum at about 600 K, and then increases to reach the set value of $T_R = 623$ K in the reaction zone. At the used values of Q_E, Q_R, and T_E the corresponding Zn vapor saturation temperature is 825 K on average, as calculated from the Zn vapor pressure[13] at the used and measured Zn weight loss. At low reaction zone temperatures (set 1), Zn vapor becomes supersaturated in the cooling zone and may form airborne Zn particles before entering the reaction zone. At high reaction zone temperatures (set 2) no supersaturation of the Zn vapor is achieved in the cooling zone, leading to particle-free Zn vapor entering the reaction zone.

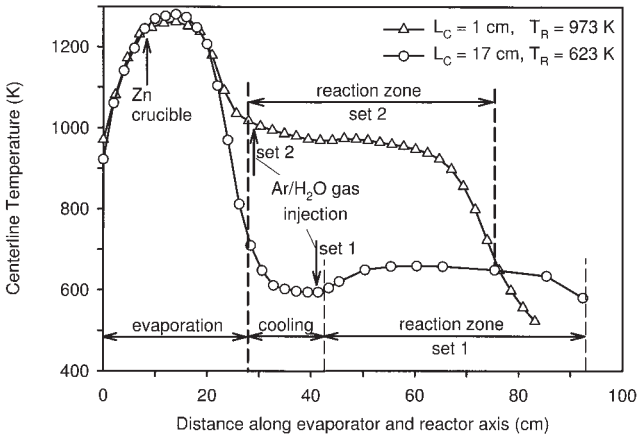

Figure 2. Temperature profiles along the evaporation, cooling, and reaction zones, representative for experimental set 1 where $L_C = 17$ cm and $T_R = 623$ K (circles); and set 2 where $L_C = 1$ cm and $T_R = 973$ K (triangles).

Zn evaporation and H_2 production

The molar rates for Zn evaporation (circles) and the corresponding H_2 production (triangles) are shown in Figure 3 as a function of process time for representative runs at $T_R = 573$ K (a: set 1) and $T_R = 923$ K (b: set 2). The process time begins as soon as Zn evaporation is detected by the loss of Zn weight from the evaporation zone (Figure 1). As expected from the same evaporation conditions for each set, the average Zn evaporation rate is similar in both sets, about 7.5×10^{-4} mol/min. The H_2 production rate follows closely the Zn evaporation rate confirming Zn hydrolysis in the aerosol reactor (Figure 3b). Because the reactor temperature is maintained above the Zn saturation temperature for set 2 (Figure 2), Zn vapor does not condense out in the gas phase. Because homogeneous hydrolysis of Zn vapor is less favored than the heterogeneous one, the measured H_2 should arise from the latter.[5] As a result, for set 2 the product H_2 may form by Zn hydrolysis on the reactor walls.[7]

For set 1 (Figure 3a) a similar synchrony in Zn evaporation and H_2 production is observed, although there is a greater difference between them compared to Figure 3b, indicating that more Zn may not react to form H_2 than in set 2. Furthermore, a shift in the start and end of H_2 production with respect to the

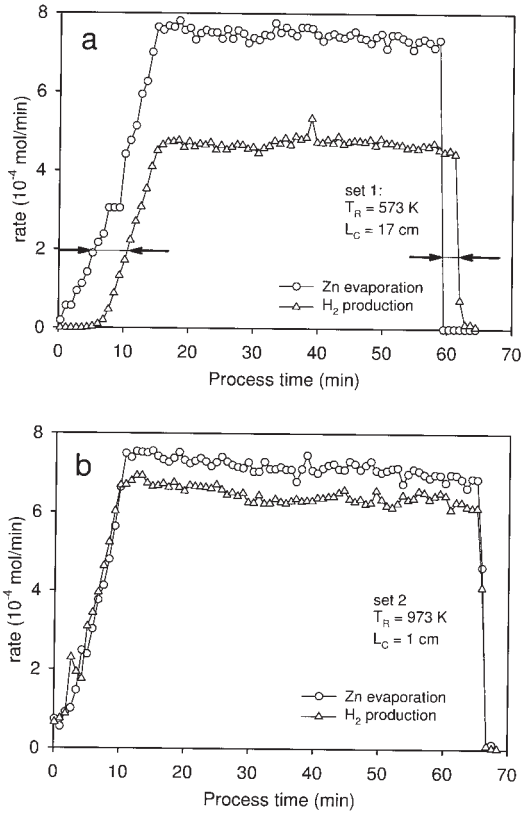

Figure 3. Molar rates of Zn evaporation (circles) and H_2 production (triangles) for two reaction temperatures T_R = 573 K (a) and T_R = 973 K (b).

The synchrony between the two rates indicates that H_2 formation takes place by Zn hydrolysis. The difference between the two rates increases with decreasing T_R as Zn particles are formed that prevent rapid Zn hydrolysis beyond their surface.

Zn evaporation is observed, as indicated by arrows. This time shift and the difference between Zn evaporation and H_2 production rates decrease with increasing T_R (not shown). In the cooling zone of set 1, the temperature drops below the Zn saturation temperature, resulting in formation of solid Zn particles. Hydrolysis of Zn particles is much slower than that on their surface.[17] As a result, the difference between Zn evaporation rate and H_2 production can be attributed to incomplete hydrolysis of Zn particles in the bulk. At increased T_R this reaction is accelerated, leading to higher H_2 conversions. Slightly different initial Zn loadings on the crucible lead to small variation in the duration of the experiment.

Particle nucleation and growth

Particle formation from Zn supersaturation in the cooling zone leads to Zn particles. Figure 4a shows a TEM image of such particles collected on the filter, produced at T_R = 573 K, which is below the saturation temperature and well below the bulk Zn melting point of 692 K.[18] Sharp-edged particles are typical for Zn particles formed below the Zn bulk melting point.[19] In the case of particle formation upon exiting the reaction zone, the particle morphology is different. Figure 4d shows the TEM image of particles produced at T_R = 1263 K. At this temperature the reaction gas is above Zn saturation temperature throughout the reaction zone, ensuring H_2 formation by Zn hydrolysis on reactor walls.[7] Because no particles are formed in the cooling and reaction zones, given that these are kept above the Zn saturation temperature, most of the Zn vapor is consumed by H_2 hydrolysis on the reactor walls. However, upon exiting the reactor, the gas temperature drops so that the remaining unreacted Zn vapor condenses out, forming filamentary particles on whose surface H_2O decomposes forming ZnO and H_2. These two extremes of particle formation span the spectrum of particle morphologies as function of reaction zone temperature. The TEM image for T_R = 723 K (Figure 4b) is dominated by hexagonal Zn particles, filamentary material (presumably from the reaction zone exit), and even rod-like ZnO particles.[10] Figure 4c shows the corresponding TEM images for T_R = 873 K where no crystalline Zn particles are visible and the image is dominated by few ZnO rod-like structures and mainly by the filamentary material typically made at rather short growth times at the end of the reaction zone. Because ZnO is unlikely to form in the gas or the solid phase in hot-wall reactors with residence times as in this study,[19] these rod-like particles have formed during the travel through the reaction zone by layer-wise deposition of Zn vapor and instantaneous oxidation by its hydrolysis.[19] Increasing the reaction zone temperature shifts the product particle morphology further to that in Figure 4d.

Product Zn/ZnO particles

For the powder collected on the filter, the d_{Zn} (triangles), d_{ZnO} (circles), and d_{BET} (squares) are plotted in Figure 5 as a function of reaction zone temperature. Data shown are only for set 1 because the amount of particles collected on the filter in set 2 was too low for BET analysis. The d_{BET} increases from

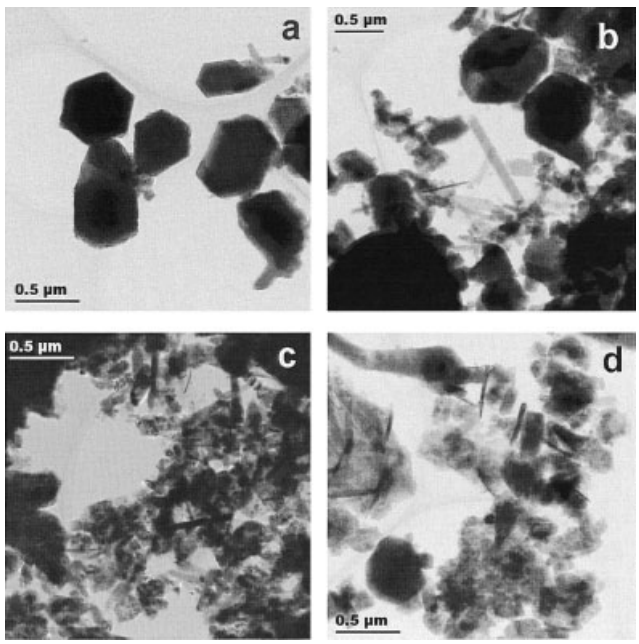

Figure 4. TEM images of Zn/ZnO powder formed at reaction zone temperatures of T_R = 573 K (a), 723 K (b), 873 K (c), and 1263 K (d) collected on a filter downstream of the reactor.

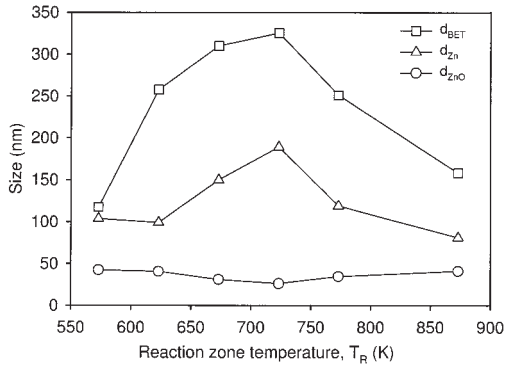

Figure 5. Sizes of Zn/ZnO particles collected on the filter as a function of reaction zone temperature, T_R.

BET equivalent particle diameter (squares) and Zn (triangles) and ZnO (circles) crystallite sizes as detected from XRD. The similar trend for d_{BET} and d_{Zn} and the relative indifference of d_{ZnO} with T_R indicates that product particle dynamics are determined by Zn particle formation by condensation–coagulation rather than by Zn hydrolysis.

117 to 325 nm at $T_R \approx 725$ K, and decreases to 158 nm at higher T_R. A similar trend is followed by the d_{Zn}, whereas d_{ZnO} is rather constant regardless of T_R. The similar trend of d_{BET} and d_{Zn} indicates that particle dynamics are determined primarily by Zn nucleation–condensation rather than by Zn hydrolysis.

The large difference between d_{BET} and d_{Zn} or d_{ZnO} indicates polycrystallinity and extended particle agglomeration, as can be observed by TEM (Figure 4). Sharp quenching of the Zn vapor below the saturation temperature at the beginning of the cooling zone (Figure 2) leads to a high number of nuclei and smaller particles,[20] mainly pure Zn as discussed with Figure 4a. Higher T_R leads to slower cooling and therefore fewer nuclei and larger particles[12] as they grow layer by layer.[21] A second mechanism leading to decreased Zn vapor concentration, and thereby fewer nuclei, may be its diffusion and deposition on the walls of the cooling zone, which, based on visual observations, increased with reaction zone temperature. Increasing T_R reduced the Zn supersaturation for nucleation and new particle formation, so Zn vapor diffused to the reactor walls.

At even higher T_R ($T_R > 700$ K for set 1), limited, if any, nucleation in cooling and reaction zones occurs and particles are mostly formed during steep cooling of the effluent gases exiting the reaction zone (Figure 2). In this case, sharp quenching leads to many nuclei that have little time to grow in this low-temperature region (Figure 4d). The evolution of the Zn crystallite size also reflects this trend (Figure 5). The fact that d_{BET} follows the trend of d_{Zn} with T_R shows that Zn particle formation and growth determine the product particle characteristics. The ZnO crystallite size (Figure 5) d_{ZnO} is much smaller than the d_{Zn} and almost constant, ranging around 42 nm at $T_R = 573$ K. This may indicate that d_{ZnO} originates from a ZnO layer covering the Zn particles supporting further ZnO formation by a surface reaction rather than by direct particle formation from the gas phase, in agreement with Weidenkaff et al.[19]

Overall H_2 conversion (X) and effective particle yield (Y)

Figure 6 shows X (triangles) and Y (circles) as well as the ZnO fraction (diamonds) as function of reaction zone temperature, T_R. The ZnO fraction is reported for set 1 only because the amount of particles collected on the filter in set 2 was too low for precise XRD analysis. For set 2, $T_R > 900$ K and $L_C = 1$ cm, only Zn vapor enters the reaction zone because the temperature of the Ar–Zn–H_2O gas is above the Zn saturation temperature of 825 K. As a result, Zn does not condense out in the reaction zone but reacts mostly on its walls, producing rather high H_2 conversions consistent with Figure 3b. Extremely low yields (≈3%) appear at these conditions that should arise from unreacted Zn vapor exiting the reaction zone, condensing out and forming Zn particles that decompose H_2O on their rather hot surfaces. These particles are rather fluffy and polycrystalline as discussed in Figures 4c and 4d. Here, limited hydrolysis, if any, takes place at the tubing walls downstream of the reaction zone, which are essentially at room temperature. Both X and Y appear insensitive to $T_R > 900$ K, indicating that chemical kinetics are limited by mass transfer, probably of Zn vapor to the reactor walls. Overall 90% of Zn was converted to ZnO, 87% at the walls and a bit less than 3% on the suspended particles, whereas 10% of Zn must have deposited on the tube walls, as was observed at the end of these experiments. Clarke and Fray[5] similarly observed an oxide-free zone followed by a mirror-like Zn coating when reactor temperatures fell below the saturation temperature ("dew point").

At 700 K $< T_R <$ 850 K and $L_C = 17$ cm (set 1), the X increases, whereas the particle ZnO content and Y decrease. As T_R decreases, ZnO hydrolysis is no longer limited by Zn mass transfer. At these conditions both large crystalline and fluffy particles are collected (Figures 4b and 4c). At sufficiently high T_R, Zn particle nucleation before reaction zone exit is prevented and H_2 formation takes place mostly heterogeneously at the reactor walls but slower than at higher T_R, as discussed above. The increased Zn vapor concentration at temperatures higher than the Zn saturation temperature[22] undergoes hydrolysis on particle surfaces and reactor walls, leading to a layer-

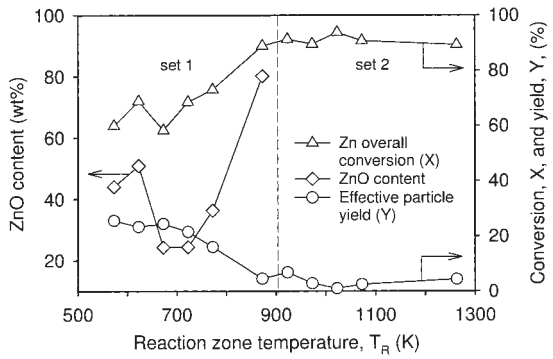

Figure 6. Overall Zn and H_2 conversion, X (triangles), effective product particle yield, Y (circles), and ZnO content (diamonds) for particles collected on the filter as a function of reaction zone temperature, T_R.

Increasing T_R favors H_2 formation as Zn hydrolysis kinetics are accelerated and limited Zn particle formation takes place.

wise buildup of the ZnO shell around the particles, as suggested by Weiss et al.[7] At the same time the hydrolysis reaction is enhanced by high T_R, resulting in high ZnO content (80 wt %). Then more unreacted Zn exits and condenses out, forming bigger Zn crystallites as indicated by XRD (Figure 5), increasing the particle yield but diminishing the ZnO content (30%) of these particles, given that ZnO is formed only at the reactor exit at rather low temperatures and short residence times. As T_R decreases further (such as 725 K), Zn particle formation takes places before or in the reaction zone, forming larger Zn crystallites (Figure 5) and the lowest ZnO content (20%) of these particles exhibiting an overall yield of about 20%. This indicates that from the overall 70% Zn converted to H_2 (Figure 6 for $T_R = 725$ K) only 4% resulted from the collected particles, whereas the remaining 66% came from Zn hydrolysis on the reaction zone walls. About 30% of the evaporated Zn was lost to the wall of the rather long cooling zone by thermophoresis and diffusion as well as downstream of the reaction zone.

At even lower T_R (<700 K) and $L_C = 17$ cm (set 1), the Y and the ZnO content increase, reaching asymptotic values as discussed for X, whereas predominantly large crystalline particles are produced with only a small fraction of fluffy ones (Figure 4a). As T_R decreases further below the Zn saturation temperature, Zn particles are formed by homogeneous nucleation before entering the reaction zone. The lower the value of T_R, the smaller the value of d_{Zn} (Figure 5), indicating increased nucleation rates (by steeper cooling) and smaller d_{BET}.[12] These freshly made Zn particles serve as sites for ZnO surface growth and H_2 formation, resulting in the highest absolute mass of ZnO particles produced from the reactor. At $T_R = 573$ K the product particles contain 40% ZnO and considering $Y = 25\%$ (Figure 6) and $X = 60\%$, the 10% of H_2 resulted from surface growth on the particles and the remaining 50% from the reactor walls. Apparently, 40% of the evaporated Zn was deposited before the reaction zone by thermophoresis and diffusion, given that no wall deposits were observed downstream of the reaction zone.

Conclusions

A hot-wall tubular quartz reactor was used to simultaneously produce H_2 and Zn/ZnO nanoparticles of various compositions by Zn metal evaporation–condensation and in-situ Zn hydrolysis. In particular, it allowed decoupling Zn evaporation from condensation hydrolysis by using two separately heated sections. Furthermore, it decoupled Zn hydrolysis from condensation by suppressing Zn condensation by operating at high reactor temperatures, above the Zn saturation temperature. The variable cooling zone length (L_C) was used to select process conditions with and without Zn particle formation before hydrolysis. The controlled reaction zone temperature (T_R) in the range of 623 to 1023 K allowed close control of the high-temperature residence time during H_2 conversion and ZnO particle formation. A synchrony between H_2 production and Zn evaporation rates showed that H_2 is indeed formed by Zn hydrolysis. Increasing the reaction zone temperature favored H_2 formation and enhanced the ZnO fraction in the product particles at the expense of particle yield. Because H_2 formation by Zn hydrolysis is favored by heterogeneous reaction, high specific surface areas or small Zn particles favor high H_2 production rates. The Zn crystallite size of 100–175 nm follows the trend of the overall BET particle size, indicating that particle characteristics are dominated by Zn nucleation, condensation, and coagulation. In contrast, the ZnO crystallite size is rather constant at about 40 nm, indicating that ZnO is formed mostly by surface reaction.

Acknowledgments

This project was funded by ETH Research Grant TH-39/04-3, the BFE–Swiss Federal Office of Energy, and the Swiss Commission of Technology and Innovation (CTI-TopNano21 Grant 6740.1 TNS). The assistance of P. Savi, B. Burg, and A. Rusconi during data collection is greatly appreciated.

Notation

d_{BET} = diameter calculated from SSA, m
d_{Zn} = Zn crystallite size, m
d_{ZnO} = ZnO crystallite size, m
L_C = cooling zone length, cm
P = overall pressure, Pa
P_{Zn} = Zn vapor pressure, Pa
$P_{Zn,S}$ = Zn saturation pressure, Pa
Q_E = carrier gas flow rate, L/min
Q_R = reaction gas flow rate, L/min
Q_{Zn} = Zn vapor flow rate (L/min) as calculated from the evaporation rate
SSA = specific surface area, m^2/g
T = temperature, K
T_E = evaporation zone temperature, K
T_R = reaction zone temperature, K
X = overall conversion, %
Y = effective particle yield, %

Greek letters

ρ_{Zn} = density of Zn, kg/m^3
ρ_{ZnO} = density of ZnO, kg/m^3
$\rho_{Zn/ZnO}$ = weighted density of Zn/ZnO particles, kg/m^3

Literature Cited

1. Steinfeld A, Kuhn P, Reller A, Palumbo R, Murray J, Tamaura Y. Solar-processed metals as clean energy carriers and water splitters. *Int J Hydrogen Energy.* 1998;23:767-774.
2. Perkins C, Weimer AW. Likely near-term solar-thermal water splitting technologies. *Int J Hydrogen Energy.* 2004;29:1587-1599.
3. Steinfeld A. Solar thermochemical production of hydrogen—A review. *Solar Energy.* 2005;78:603-315.
4. Lewis NL, Basic research needs for solar energy utilization. Office of Science of the US Department of Energy; 2005. May be accessed at www.sc.doe.gov/bes/reports/files/SEU_rpt.pdf
5. Clarke JA, Fray DJ. Oxidation of zinc vapour by hydrogen-water vapour mixtures. *Trans Inst Mining Metall C.* 1979;88:C161-C166.
6. Berman A, Epstein M. The kinetics of hydrogen production in the oxidation of liquid zinc with water vapor. *Int J Hydrogen Energy.* 2000;25:957-967.
7. Weiss RJ, Ly HC, Wegner K, Pratsinis SE, Steinfeld A. H_2 production by Zn hydrolysis in a hot-wall aerosol reactor. *AIChE J.* 2005;51:1966-1970.
8. Kischkewitz J, Woditsch P, Westerhaus A, Griebler W-D, Liedekerke MD. Pigments, inorganic, 2.3 zinc oxide. In: *Ullmann's Encyclopedia of Industrial Chemistry*. Weinheim, Germany: Wiley-VCH Verlag GmbH; 2002.
9. Wegner K, Pratsinis SE. Scale-up of nanoparticle synthesis in diffusion flame reactors. *Chem Eng Sci.* 2003;58:4581-4589.
10. Wang ZL. Zinc oxide nanostructures: Growth, properties and applications. *J Phys Condens Matter.* 2004;16:R829-R858.
11. Tani T, Madler L, Pratsinis SE. Homogeneous ZnO nanoparticles by flame spray pyrolysis. *J Nanoparticle Res.* 2002;4:337-343.
12. Wegner K, Walker B, Tsantilis S, Pratsinis SE. Design of metal

nanoparticle synthesis by vapor flow condensation. *Chem Eng Sci.* 2002;57:1753-1762.
13. Yaws CL. *Chemical Properties Handbook*. New York, NY: McGraw-Hill; 1999.
14. Swanson HE, Tatge E. Standard X-ray diffraction patterns. *J Res Natl Bur Stand.* 1951;46:318-327.
15. Schulz H, Thiemann KH. Structure parameters and polarity of the wurtzite type compounds SiC–2H and ZnO. *Solid State Commun.* 1979;32:783-785.
16. Cheary RW, Coelho AA. Axial divergence in a conventional X-ray powder diffractometer. I. Theoretical foundations. *J Appl Crystallogr.* 1998;31:851-861.
17. Bazan JC, Gschaider ME, Alimenti GA. Gravimetric study of interaction of water vapour with metallic zinc. *J Therm Anal Calorim.* 1999;55:569-579.
18. Perry RH, Green DW. *Perry's Chemical Engineers' Handbook*. New York, NY: McGraw-Hill; 1997.
19. Weidenkaff A, Steinfeld A, Wokaun A, Auer PO, Eichler B, Reller A. Direct solar thermal dissociation of zinc oxide: Condensation and crystallisation of zinc in the presence of oxygen. *Solar Energy.* 1999; 65:59-69.
20. Panda S, Pratsinis SE. Modeling the synthesis of aluminum particles by evaporation–condensation in an aerosol flow reactor. *Nanostruct Mater.* 1995;5:755-767.
21. Wang ZL, Harris R. Morphology of zinc deposited from mixed gas streams at reduced pressures. *Mater Charact.* 1993;30:155-173.
22. Backman U, Jokiniemi JK, Auvinen A, Lehtinen KEJ. The effect of boundary conditions on gas-phase synthesised silver nanoparticles. *J Nanoparticle Res.* 2002;4:325-335.

Manuscript received Dec. 6, 2005, and revision received May 5, 2006.